

## REFERENCES AND NOTES

- M. J. Fletcher and D. R. Sanadi, *Biochem. Biophys. Acta* **51**, 356 (1961).
- J. F. Dice and A. L. Goldberg, *Proc. Natl. Acad. Sci. U.S.A.* **72**, 3893 (1975); S. M. Russell, R. J. Burgess, R. J. Mayer, *Biochem. J.* **256**, 8652 (1980).
- A. L. Goldberg, *Eur. J. Biochem.* **203**, 9 (1992).
- E. Kutejová, G. Durčová, E. Surovková, Š. Kužela, *FEBS Lett.* **329**, 47 (1993).
- S. A. Goff and A. L. Goldberg, *Cell* **41**, 587 (1985).
- D. T. Chin, S. A. Goff, T. Webster, T. Smith, A. L. Goldberg, *J. Biol. Chem.* **263**, 11718 (1988); K. Ito, S. Uda, H. Yamagata, *J. Bacteriol.* **174**, 2281 (1992); N. Tojo, S. Inouye, T. Komano, *ibid.* **175**, 2271 (1993); N. Wang, S. Gottesman, M. C. Willingham, M. M. Gottesman, M. Maurizi, *Proc. Natl. Acad. Sci. U.S.A.* **90**, 11247 (1993).
- Two degenerate oligonucleotide primers were synthesized: 5'-GTI(T/C)TGAIGA(A/G)GA(T/C)-CA(T/C)TA(T/C)GG-3' and 5'-GA(T/C)TC(T/C)-TTCATACITCICCA(A/G)(T/C)TG-3'. The first is a 32-fold degenerate 23-nucleotide oligomer in the sense direction, corresponding to amino acids 490 to 497 of the human Lon protein. The second is a 16-fold degenerate 26-nucleotide oligomer in the antisense direction, corresponding to amino acids 809 to 817 of the human Lon protein. PCR was carried out in a total volume of 100  $\mu$ l, in the presence of 2.5 mM MgCl<sub>2</sub>, 1 to 2  $\mu$ M primers, and either 0.4  $\mu$ g of a yeast cDNA library [H. Liu, J. Krizek, A. Bretscher, *Genetics* **132**, 665 (1992)] or DNA from a single yeast colony. A fragment of ~1.2 kb was amplified from both templates, gel-isolated, ligated into a TA cloning vector (Invitrogen, San Diego, CA), and sequenced by the dideoxy method.
- The 1.2-kb PCR fragment was <sup>32</sup>P-labeled by random priming to a specific activity of ~4 × 10<sup>8</sup> counts per minute (cpm) per microgram of DNA. This probe was used to screen 50,000 colonies of a cDNA library. Positive colonies were purified by rescreening.
- A 745-bp Eco RV-Nae I fragment from within the *LON* gene was replaced by a blunted 3.0-kb Bgl II fragment carrying the yeast *LEU2* gene. A Hind III-Xba I fragment containing the *LEU2* gene flanked by 0.2 kb and 1.0 kb of the *LON* gene was purified by gel electrophoresis and used to transform the diploid yeast strain YKB5 (*MATa**MATa* *ura3/ura3*, *his4/his4*, *leu2/leu2*, *lys2/LYS2*, *ade2/ADE2*) to leucine prototrophy [D. Gietz, A. St. Jean, R. A. Woods, R. H. Schiestl, *Nucleic Acids Res.* **20**, 1425 (1992)]. Chromosomal DNA from transformants was digested with Hind III and Xba I and probed with a random-primed fluorescently labeled Hind III-Xba I fragment by Southern (DNA) blotting (ECL Random Prime Labelling System, Amersham, Buckinghamshire, England).
- C. K. Suzuki and G. Schatz, unpublished data.
- B. Dujon, in *The Molecular Biology of the Yeast Saccharomyces: Life Cycle and Inheritance*, J. N. Strathern *et al.*, Eds. (Cold Spring Harbor Laboratory, Cold Spring Harbor, NY, 1981), p. 505.
- M. Desautels and A. L. Goldberg, *Proc. Natl. Acad. Sci. U.S.A.* **79**, 1869 (1982); *J. Biol. Chem.* **257**, 11673 (1982).
- LON* cells were converted to  $\rho^-$  mutants by growth in the presence of acriflavin (20  $\mu$ g/ml). The presence of mtDNA was ascertained by staining of the cells with DAPI, and respiratory deficiency by inability to grow on rich medium containing ethanol and glycerol as carbon sources.
- LON*  $\rho^-$  and *lon::LEU2* cells were grown in YPGal (1% yeast extract, 2% peptone, 2% galactose) at 30°C and harvested during log phase growth. Mitochondria were isolated as described [G. Daum, S. M. Gasser, G. Schatz, *J. Biol. Chem.* **257**, 13075 (1982)], except that the phenylmethylsulfonyl fluoride in the isolation medium was replaced by 1 mM each of TLCK and TPCK. The mitochondria were converted to mitoplasts by osmotic shock [B. S. Glick *et al.*, *Cell* **69**, 809 (1992)]. Matrix contents were released from mitoplasts by sonication on ice and centrifuged at 100,000g for 5 min at 4°C. The supernatant was loaded onto a Q-Sepharose Fast Flow ion exchange column (0.5 ml bed volume) equilibrated with buffer A [20 mM Tris-HCl (pH 8.0), 0.1 mM EDTA, 1 mM dithiothreitol, 10% glycerol]. Casein (100  $\mu$ g) was radiolabeled with 100  $\mu$ Ci of carrier-free Na<sup>125</sup>I by the chloramine-T method [F. C. Greenwood, W. M. Hunter, J. S. Glover, *Biochem. J.* **89**, 114 (1963)]; the specific radioactivity of the radioactively labeled casein was adjusted with unlabeled casein to 30  $\mu$ Ci per milligram of casein. Proteolysis was assayed as described by Y. Katayama, S. Gottesman, and M. R. Maurizi [*J. Biol. Chem.* **262**, 4477 (1987)]. In the presence of 2 mM ATP, matrix fractionated from *LON* mitoplasts released 12,000 ± 290 cpm of acid-soluble <sup>125</sup>I-peptides; in the absence of added ATP, 5700 ± 157 cpm were released. With matrix fractionated from *lon::LEU2* mitoplasts, the corresponding values were 5600 ± 1184 cpm and 4254 ± 192 cpm, respectively.
- B. Stevens, in (11), p. 471.
- L. Van Dyck, D. A. Pearce, F. Sherman, *J. Biol. Chem.* **269**, 238 (1994).
- M. P. Yaffe and G. Schatz, *Proc. Natl. Acad. Sci. U.S.A.* **81**, 4819 (1984).
- We thank R. D. Klausner for support during the cloning of the yeast *LON* gene; S. Gottesman, M. M. Gottesman, and M. Maurizi for transmitting data before publication and for reviewing this manuscript; and A. Bretscher (Cornell University, Ithaca, NY) for providing colonies of a yeast cDNA library. We are grateful to U. Sauder and M. Duerrenberger (Biozentrum) for technical assistance with the electron microscopy. Supported by grant 3-26189.89 to G.S. from the Swiss National Science Foundation, by a grant from the European Community Human Capital and Mobility Program, and by a postdoctoral fellowship to C.K.S. from the Damon Runyon-Walter Winchell Cancer Research Foundation.

22 November 1993; accepted 7 February 1994

## Soluble $\beta$ -Amyloid Induction of Alzheimer's Phenotype for Human Fibroblast K<sup>+</sup> Channels

René Etcheberrigaray, Etsuro Ito,\* Christopher S. Kim, Daniel L. Alkon†

Although  $\beta$ -amyloid is the main constituent of neurite plaques and may play a role in the pathophysiology of Alzheimer's disease, mechanisms by which soluble  $\beta$ -amyloid might produce early symptoms such as memory loss before diffuse plaque deposition have not been implicated. Treatment of fibroblasts with  $\beta$ -amyloid (10 nM) induced the same potassium channel dysfunction previously shown to occur specifically in fibroblasts from patients with Alzheimer's disease—namely, the absence of a 113-picosiemens potassium channel. A tetraethylammonium-induced increase of intracellular concentrations of calcium, [Ca<sup>2+</sup>]<sub>i</sub>, a response that depends on functional 113-picosiemens potassium channels, was also eliminated or markedly reduced by 10 nM  $\beta$ -amyloid. Increased [Ca<sup>2+</sup>]<sub>i</sub> induced by high concentrations of extracellular potassium and 166-picosiemens potassium channels were unaffected by 10 nM  $\beta$ -amyloid. In Alzheimer's disease, then,  $\beta$ -amyloid might alter potassium channels and thus impair neuronal function to produce symptoms such as memory loss by a means other than plaque formation.

The protein  $\beta$ -amyloid ( $\beta$ AP) is implicated as a key factor in the pathophysiology of Alzheimer's disease (AD) (1, 2). It is the main component of the neurite plaques which, together with the neurofibrillary tangles, constitute the neuropathological features that confirm AD (3). Mutations of the amyloid precursor protein (APP), from which  $\beta$ AP originates, are present in a limited number of AD cases (1 to 5%) (4), and altered APP processing has been proposed to result in the generation of amyloidogenic protein fragments (5).

Soluble  $\beta$ AP can be the product of normal

proteolytic processing (2, 6), whereas an excess of  $\beta$ AP is released from a mutant APP (7). Proposed mechanisms for  $\beta$ AP's deleterious effects include direct neurotoxicity (8, 9), induction of calcium metabolism derangements leading to enhanced excitotoxicity (10), membrane permeability enhancement (11), and formation of Ca<sup>2+</sup> channels that would lead to abnormally high cytosolic Ca<sup>2+</sup> concentrations and subsequently cell death (12). Nevertheless, mechanisms by which  $\beta$ AP causes symptoms such as memory loss without plaque formation have not been implicated.

A 113-pS tetraethylammonium (TEA)-sensitive K<sup>+</sup> channel is functionally absent in fibroblasts from AD patients (13). As a consequence, the increase in [Ca<sup>2+</sup>]<sub>i</sub> observed after depolarization induced by TEA in fibroblasts derived from control individuals [including fibroblasts from young individuals (YC), age-matched individuals (AC), and

Laboratory of Adaptive Systems, National Institute of Neurological Disorders and Stroke, Room B-205, Building 36, National Institutes of Health, Bethesda, MD 20892, USA.

\*Present address: Laboratory of Animal Behavior and Intelligence, Division of Biological Sciences, Graduate School of Science, Hokkaido University, Sapporo 060, Japan.

†To whom correspondence should be addressed.

patients with non-Alzheimer's neurological or psychiatric conditions] was absent in all fibroblast cell lines examined from patients with familial and nonfamilial cases of AD (13). Inositol trisphosphate ( $IP_3$ )-mediated  $Ca^{2+}$  release from intracellular stores is enhanced in fibroblasts from AD patients (14). Related changes of  $K^+$  channels and  $Ca^{2+}$  responses have been observed in olfactory neuroblasts from AD patients (15). Because  $\beta$ AP may contribute to the pathogenesis of AD and is produced by AD fibroblasts (16), we studied the effects of this peptide on  $K^+$  channel function and  $Ca^{2+}$  release in human fibroblasts.

Human fibroblasts were obtained from the Coriell Cell Repositories and cultured as described (13, 14, 17). Patches (cell-attached) (13, 17, 18) were obtained in 21 cells from five different AC cell lines treated with  $\beta$ AP (10 nM) for 48 hours. The 113-pS  $K^+$  channel was absent in all but one of the treated cells (5%), whereas it was found in 16 out of 17 untreated cells (94%) (13) from the same five AC lines ( $P < 0.0001$ , Fisher's exact test) (Fig. 1). By contrast, another  $K^+$  channel of 166 pS that is present with the same frequency in control and AD fibroblasts (13) was present with equal frequency in patches from AC cell lines treated with or without  $\beta$ AP ( $\chi^2 = 1.89$ , not significant) (Fig. 1). Thus  $\beta$ AP appears to selectively impair the same  $K^+$  channel that is func-

tionally absent in fibroblasts from AD patients.

To further test this possibility, we used fluorescent imaging (19) with the  $Ca^{2+}$ -sensitive dye fura 2-AM to assess  $[Ca^{2+}]_i$  after blockade of the 113-pS  $K^+$  channels with TEA, which in turn causes cell depolarization and calcium entry (13, 14, 17). The application of  $\beta$ AP (10 nM) did not change basal  $[Ca^{2+}]_i$  in 11 cell lines examined {treated =  $80 \pm 2.2$  nM (mean  $\pm$  SD), untreated =  $77.5 \pm 2.7$  nM, dimethyl sulfoxide (DMSO) alone =  $79.7 \pm 2.7$  nM (10 cell lines),  $P > 0.05$  [analysis of variance (ANOVA) Bonferroni posttest]}. These concentrations are also identical to the concentrations measured in 43 different cell lines of AD and control groups (13, 14). In contrast, incubation of cells with a higher concentration of  $\beta$ AP (1  $\mu$ M) caused a small but significant elevation of basal  $[Ca^{2+}]_i$  in AD and control fibroblasts [treated =  $118.6 \pm 2.4$  nM ( $n = 8$  cell lines), nontreated =  $77.5 \pm 1.1$  nM ( $n = 8$  cell lines),  $P < 0.0001$  ( $t$  test)] (Fig. 2). The TEA-induced increase in  $[Ca^{2+}]_i$  was completely abolished for six out of eight control cell lines treated with  $\beta$ AP (10 nM) (total number of cells tested = 194,  $P < 0.005$ , Fisher's exact test) compared with the same eight untreated cell lines. In the two cell lines treated with  $\beta$ AP (10 nM) that had some response, the increase in  $[Ca^{2+}]_i$  in response to TEA was significantly lower after treatment

than in untreated controls ( $P < 0.001$ ,  $t$  test) (Fig. 3). Incubation (48 hours) with 1  $\mu$ M  $\beta$ AP also eliminated or greatly reduced the TEA response in control fibroblasts ( $n = 8$  cell lines,  $n = 194$  cells). Treatment with DMSO alone (six cell lines,  $n = 146$  cells) did not affect the TEA response. Increased  $[Ca^{2+}]_i$  induced by depolarization with 50 mM external KCl, observed in fibroblasts from AD patients as well as in cells from control individuals (13), was unaffected by 10 nM  $\beta$ AP in both AD and control (YC and AC) fibroblasts. After treatment with 10 nM  $\beta$ AP, the  $K^+$  response was preserved in six out of eight control cell lines and in two out of three AD lines, which is not significantly different in comparison with responses of the same untreated cell lines ( $P = 0.21$ , Fisher's exact test). Responses to 50 mM KCl were slightly, but not significantly, higher in YC fibroblasts (treated) as compared with responses in AC and AD cell lines that had been treated with 10 nM  $\beta$ AP ( $P = 0.24$ , ANOVA). No significant differences for the KCl response were observed between treated AC and untreated AC lines, nor were there differences between the treated AD and untreated AD lines. Moreover, when KCl responses of all treated cell lines ( $n = 11$ ) were compared with responses of all cell lines left untreated ( $n = 11$ ,  $P = 0.21$ ,  $t$  test) or treated with DMSO alone ( $n = 4$ ,  $P = 0.5$ ,  $t$  test),

**Fig. 1.** Cell-attached recordings in human fibroblasts. (A) Sample traces of the 113-pS  $K^+$  channel. This channel was not detected when AC fibroblasts were treated with  $\beta$ AP (1–40) (10 nM) (bottom trace). Upward deflections represent channel closures. (B) The  $K^+$  channel with larger conductance (166 pS) in AC cell lines was unaffected by  $\beta$ AP treatment (bottom trace). The 113-pS channel was open about 60% of the time in control cell lines compared with ~10% for the 166-pS channel present in control (AC and YC), AD, and  $\beta$ AP-treated (10 nM) AC cell lines. (C) The 113-pS channel was present in only 1 of 21 cells (five cell lines of treated controls, middle column). This channel, however, was present in 94% of the previously recorded untreated controls (five different cell lines, 17 cells examined). Untreated control observations were also repeated and confirmed. This is almost identical to the situation in AD fibroblasts (right symbol), where no 113-pS channel was observed (27 cells from nine cell lines). Much of the data for untreated control (YC and AC) and AD cell lines had been collected before this study (13).

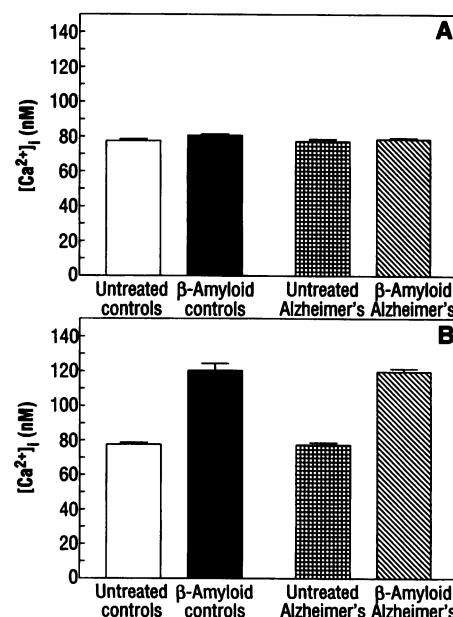
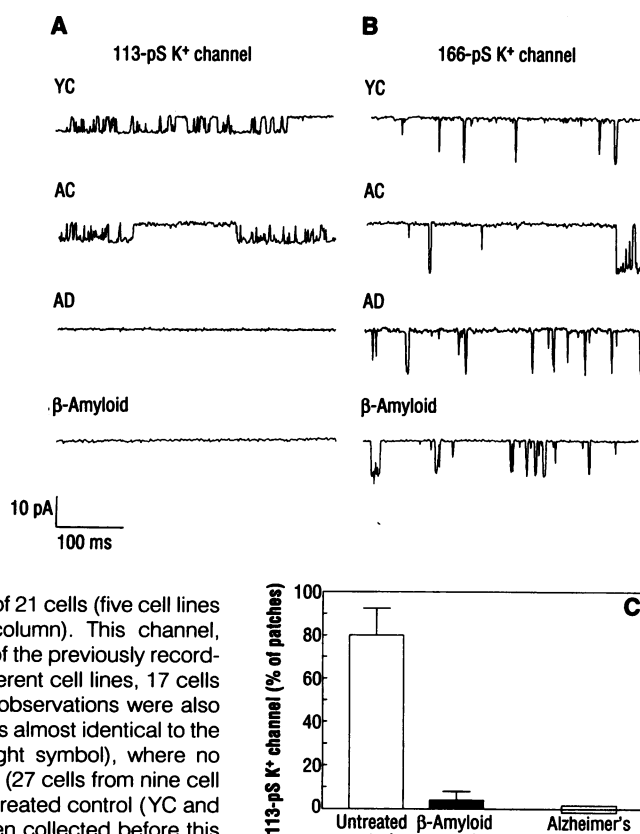


**Fig. 2.** Basal  $Ca^{2+}$  concentrations in human fibroblasts. (A) Resting  $Ca^{2+}$  concentrations were unchanged by 10-nM  $\beta$ AP treatment. Concentrations were identical in untreated and treated controls (eight different cell lines each) as well as in AD cell lines (three AD treated and four untreated lines). (B) In contrast to 10 nM, 1  $\mu$ M  $\beta$ AP significantly ( $P < 0.0001$ ,  $t$  test) elevated basal  $Ca^{2+}$  concentrations in treated controls (four cell lines, 259 cells) and in treated AD lines (four cell lines, 274 cells).

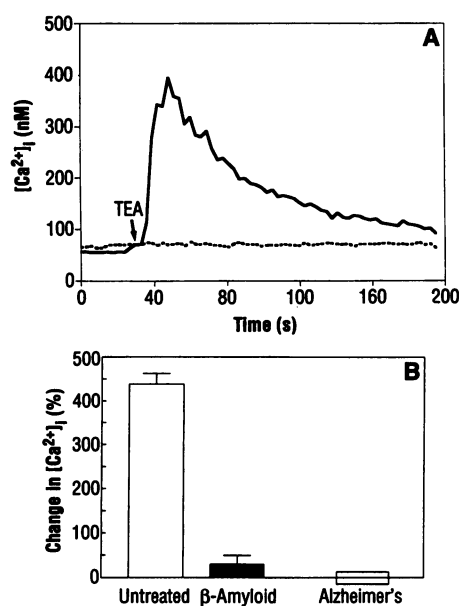


**Fig. 3.** Effects of 10 nM  $\beta$ AP on the TEA response. (A) Typical time course representation of the TEA-induced  $\text{Ca}^{2+}$  elevation in control cells (solid line), where peak ( $\approx 400$  nM) is reached  $\approx 15$  s after application of 100 mM TEA (indicated by the arrow). The dashed line illustrates the effect of  $\beta$ AP on the same control cell preparation. Each line is the averaged response of seven cells simultaneously measured. (B) Bar graph of the percent change (from resting  $\text{Ca}^{2+}$  concentrations) shows the virtual elimination of the TEA response in treated control cells (eight cell lines, 194 cells), similar to observations for AD fibroblasts (four cell lines, 285 cells measured). Preparations of the various cell lines were tested for response to TEA in the absence (left) or presence (center) of  $\beta$ AP. The responses of AD fibroblasts shown here are in agreement with our previous report showing no responses in 13 different AD lines ( $> 700$  cells measured) (13).

there were no statistically significant differences between the groups. These results further indicate that  $\beta$ AP selectively affects the 113-pS  $\text{K}^+$  channel, not voltage-dependent  $\text{Ca}^{2+}$  channels, to cause the loss of the TEA response in YC and AC fibroblasts as was observed for TEA responses of AD fibroblasts.

There were no effects of 10 nM  $\beta$ AP on the increase in  $[\text{Ca}^{2+}]_i$  induced by bombesin, which does not depend on external  $\text{Ca}^{2+}$  and does not require depolarization or blockade of  $\text{K}^+$  channels (14). The increase in  $[\text{Ca}^{2+}]_i$  induced by bombesin was found to be greater in AD cell lines (14) than in control (YC and AC) cell lines ( $P < 0.02$ ,  $t$  test) (Fig. 4). The lack of a  $\beta$ AP effect on the bombesin response suggests that bombesin-induced  $\text{Ca}^{2+}$  release becomes deranged with AD before cellular dysfunction caused by soluble  $\beta$ AP or independent of it (or both). Alternatively, the bombesin response might change at a more advanced stage when generalized cell damage, including  $\beta$ AP deposition and plaque formation, occurs.

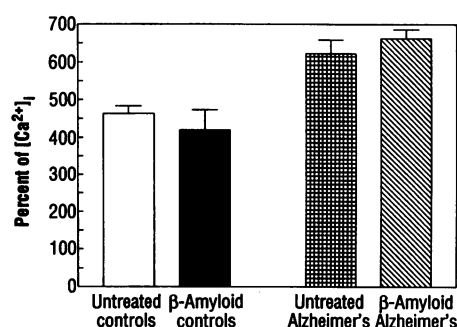


**Fig. 4.** Bombesin-induced increases in  $[\text{Ca}^{2+}]_i$  were unchanged for control cells (four cell lines, 91 cells) treated with  $\beta$ AP and AD cells treated with  $\beta$ AP (two cell lines, 30 cells).

The concentration of  $\beta$ AP (10 nM) that produced AD-specific changes in  $\text{K}^+$  channel function similar to changes observed for cells from AD patients was lower than concentrations found to cause alteration of  $\text{Ca}^{2+}$  homeostasis or toxicity (8–10). Mattson *et al.* (10) reported that enhanced glutamate toxicity was observed when cells were treated with  $\beta$ AP concentrations between 20 to 80  $\mu\text{M}$  (from aqueous stock solutions), and that concentrations of 10  $\mu\text{M}$  or below had virtually no effect on glutamate toxicity. In addition, potentiation of  $\text{Ca}^{2+}$  ionophore toxicity was observed at 5  $\mu\text{M}$  as was elevation of resting  $\text{Ca}^{2+}$  concentrations at 2  $\mu\text{M}$   $\beta$ AP. With 1  $\mu\text{M}$   $\beta$ AP we observed increases in  $[\text{Ca}^{2+}]_i$  that could cause cell damage. Furthermore, in reports of neurotrophic and toxic effects (9), longer (4 days)  $\beta$ AP incubation periods were used rather than the 48 hours used in the present study. In frog sympathetic neurons, 30  $\mu\text{M}$   $\beta$ AP caused a nonspecific increase in membrane conductance. Similar increases in conductance or membrane permeability have also been observed in PC12 cells (11), but no specific ions or current carriers were identified.

Thus, it is possible that soluble  $\beta$ AP might contribute to AD pathophysiology by causing  $\text{K}^+$  channel dysfunction. If  $\text{K}^+$  channel dysfunction occurs in central nervous system neurons as we have found for fibroblasts (13) and olfactory neuroblasts (15), it might affect brain functions such as memory storage, which has been found to involve long-term changes of  $\text{K}^+$  channels (20).

## REFERENCES AND NOTES

1. D. J. Selkoe, *Neuron* 6, 487 (1991); C. L. Joachim and D. J. Selkoe, *Alzheimer Dis. Assoc. Disord.* 6, 7 (1992).
2. D. J. Selkoe, *Trends Neurosci.* 16, 403 (1993).
3. R. Katzman, *N. Engl. J. Med.* 314, 964 (1986); A. I. Bush, K. Beyreuther, C. L. Masters, *Pharmacol. Ther.* 56, 97 (1992).
4. R. E. Tanzi *et al.*, *Am. J. Hum. Genet.* 51, 273 (1992); J. Johnston *et al.*, *Hum. Molec. Genet.* 2, 1045 (1993); P. St George-Hyslop, personal communication.
5. S. S. Sisodia, E. H. Koo, K. Beyreuther, A. Unterbeck, D. L. Price, *Science* 248, 492 (1990); S. Estus

- et al.*, *ibid.* 255, 726 (1992); T. E. Golde, S. Estus, L. H. Younkin, D. J. Selkoe, S. G. Younkin, *ibid.*, p. 728; C. Haass, E. H. Koo, A. Mellon, A. Y. Hung, D. J. Selkoe, *Nature* 357, 500 (1992).
6. M. Shoji *et al.*, *Science* 258, 126 (1992); C. Haass *et al.*, *Nature* 359, 322 (1992); J. Busciglio, D. H. Gabuzda, P. Matsudaira, B. A. Yankner, *Proc. Natl. Acad. Sci. U.S.A.* 90, 2092 (1993).
7. X.-D. Cai, T. E. Golde, S. G. Younkin, *Science* 259, 514 (1993).
8. B. A. Yankner *et al.*, *ibid.* 245, 417 (1989); J. S. Whitson and S. H. Appel, *Soc. Neurosci. Abstr.* 19, 1250 (1993).
9. B. A. Yankner, L. K. Duffy, D. A. Kirschner, *Science* 250, 279 (1990).
10. M. P. Mattson *et al.*, *J. Neurosci.* 12, 376 (1992); M. P. Mattson *et al.*, *Trends Neurosci.* 16, 409 (1993).
11. M. A. Simmons and C. R. Schneider, *Neurosci. Lett.* 150, 133 (1993); Z. Galdzicki *et al.*, *Soc. Neurosci. Abstr.* 19, 397 (1993).
12. N. Arispe, E. Rojas, H. B. Pollard, *Proc. Natl. Acad. Sci. U.S.A.* 90, 567 (1993).
13. R. Etcheberrigaray *et al.*, *ibid.*, p. 8209.
14. E. Ito *et al.*, *ibid.* 91, 534 (1994).
15. R. Etcheberrigaray *et al.*, in preparation.
16. G. M. Cole, K. Mak, J. Wu, S. A. Frautschy, *Soc. Neurosci. Abstr.* 19, 1275 (1993).
17. Procedures for cell culture are as follows. Human skin fibroblasts were seeded and maintained as described (13). Cells from four YC individuals [GM03377, GM03652, GM04390, and GM08399; two males and two females;  $21.25 \pm 2.63$  years of age (mean  $\pm$  SD)], four AC individuals [GM04260, AG04560, AG08044, and AG09878; two males and two females;  $59.5 \pm 1.29$  years of age], and four AD patients [AG06848, AG08170, AG07376, and AG08243; two males and two females;  $60.5 \pm 7.85$  years of age] were used. There are no differences in growth rates or time to senescence between AD and control fibroblasts (13, 14, 21). Neither elicited increases in  $[\text{Ca}^{2+}]_i$ , nor basal  $[\text{Ca}^{2+}]_i$ , are correlated with the passage number of the cells (14, 22). The  $\beta$ AP (1–40) (Bachem, Torrance, CA) was initially dissolved in DMSO (1 mM) (10) and further diluted in saline solution to the desired final concentration (1  $\mu\text{M}$  or 10 nM) just before application. The  $\beta$ AP was added 24 hours after seeding, and all experiments were done 48 hours after addition of  $\beta$ AP. Procedures for electrophysiology and single-channel analysis are as follows. Patch-clamp experiments were done at  $21^\circ$  to  $23^\circ\text{C}$  as described (13, 18). Before recordings were made, culture medium was replaced with a solution containing 150 mM NaCl, 5 mM KCl, 2 mM  $\text{CaCl}_2$ , 1 mM  $\text{MgCl}_2$ , and 10 mM Hepes (pH 7.4). Pipettes were made from Blue Tip capillary tubes (inner diameter of 1.1 to 1.2 mm) with a BB-CH Mecanex puller and then filled with  $\text{K}^+$  solution containing 140 mM KCl, 2 mM  $\text{CaCl}_2$ , 1 mM  $\text{MgCl}_2$ , and 10 mM Hepes (pH 7.4). Pipette resistances were between 6 to 8 Mohm. Records were obtained with an Axopatch-1C amplifier (dc of 10 kHz), stored on tape (Toshiba PCM video recorder), and transferred to a personal computer with an Axolab interface. All recordings lasted for at least 10 min. The pClamp suite of programs was used for single-channel data acquisition and analysis. Amplifier, interface, and software were obtained from Axon Instruments (Foster City, CA). Procedures for calcium imaging are as follows. The cells were incubated with fura 2-AM (2  $\mu\text{M}$ ) in basal salt solution (BSS), 140 mM NaCl, 5 mM KCl, 2.5 mM  $\text{CaCl}_2$ , 1.5 mM  $\text{MgCl}_2$ , 5 mM glucose, and 10 mM Hepes (pH 7.4) at room temperature for 60 min. After three washes with BSS, the cells were used for  $[\text{Ca}^{2+}]_i$  determinations. Cell fluorescence was measured with a  $\text{Ca}^{2+}$ -imaging system (Hamamatsu Photonics ARGUS 50, Hamamatsu, Japan). For excitation, 340- and 380-nm bandpass filters with a neutral-density filter were used. Images of fluorescence were obtained with a 400-nm dichroic mirror and a 510-nm long-pass barrier filter. The objective lens was a 10 $\times$  Nikon UV fluor, and only one-fourth of a whole image was recorded to avoid uneven illumination. The averaged  $\text{Ca}^{2+}$  responses within 15 by 15 pixels in cytosolic cellular compartments obtained were quantified with ratios of fluorescence

emitted at 510 nm with activation at 340 nm to fluorescence emitted at 510 nm with activation at 380 nm. After calibration, the ratio values were transformed to absolute  $[Ca^{2+}]$ , values with the following equation:  $R = R_{\max} + (R_{\min} - R_{\max}) / (1 + ([Ca^{2+}]/K_d)^b)$ , where  $R$  denotes F340/F380,  $R_{\max}$  and  $R_{\min}$  are the values of  $R$  when the concentration of  $Ca^{2+}$  is at a maximum and a minimum, respectively, and  $K_d$  is the dissociation constant of fura 2-AM for  $Ca^{2+}$  (240 nM). The value of  $b$ , which determines the degree of asymmetry, was 1.2. TEA was added by perfusion of 5 ml of a modified BSS

solution containing 100 mM TEA and low NaCl (50 mM). Other components were not changed (see above for BSS composition). Bombesin was applied by addition of 1 ml of BSS plus 2  $\mu$ M bombesin to a dish containing 1 ml of BSS (final bombesin concentration = 1  $\mu$ M). Solution were applied within 0.5 cm of the cells whose responses were measured.

20. D. L. Alkon, *Sci. Am.* **260**, 42 (1989).
21. G. Tesco, M. Vergelli, L. Amaducci, S. Sorbi, *Exp. Gerontol.* **28**, 51 (1993).
22. L. A. Borden, F. R. Maxfield, J. E. Goldman, M. L. Shelanski, *Neurobiol. Aging* **13**, 33 (1991).
23. We thank Hamamatsu Photonics Corporation that generously provided the  $Ca^{2+}$ -imaging equipment used in this study. We also thank J. Schwartz for the use of the cell culture facility.

29 November 1993; accepted 10 February 1994

## TECHNICAL COMMENTS

### High-Pressure Melting of (Mg,Fe)SiO<sub>3</sub>-Perovskite

We commend Zerr and Bohler on their high-pressure melting study of Mg-silicate perovskite (1). However, we disagree with their interpretation of earlier studies and their own experiments.

Contrary to what Zerr and Bohler state (1, p. 554), we have previously visually observed the melting of perovskite and other materials in situ at high pressures and temperatures (2–8), including forced convection across molten zones of about 5 to 30  $\mu$ m in diameter, similar to that described by Zerr and Bohler. We also determined temperature variations across our samples, both experimentally and theoretically (3, 9, 10).

Zerr and Bohler state that the melting data of Jeanloz and co-workers (4, 11) "are in strong contradiction to" more recent measurements by Sweeney and Heinz (12). This suggests a lack of reproducibility among the earlier experiments. Yet, there is no contradiction, as Sweeney and Heinz explained that their "data do not represent the true melting temperature of iron-magnesium-silicate perovskite" (13). Instead, Sweeney and Heinz reported average field-of-view temperatures across their samples for which the correlation between laser power and measured temperature showed a break in slope (12). In general, it is not known how precisely the correlation of laser power and (average) temperature reproduces melting temperatures obtained using other criteria, but it is known that the average temperatures reported by Sweeney and Heinz must be far below the true melting temperature; hence, their cautionary note. Indeed, when a first-order correction is applied for the difference between average and peak temperatures within the sample, Sweeney and Heinz find relatively good agreement with the earlier studies (that is, within mutual uncertainties) over the pressure range examined by Zerr and Bohler.

A critical issue not addressed by Zerr and Bohler is the nature of the temperature gradients across their samples. That there must be gradients is well established, both empirically and theoretically, for any laser

heating experiment in the diamond cell (9, 10). This is equally true for a Nd:YAG (3, 6, 8, 9) or a CO<sub>2</sub> (14, 15) heating laser because the intensity distribution across a laser beam is Gaussian, resulting in a spatially variable heat source within a sample (16). Also, diamonds represent nearly infinite and perfect heat sinks because of their dimensions (17) and because of the high thermal conductivity of diamond. Therefore, the nonuniformity of both heat sources and heat sinks must inevitably produce three-dimensional temperature gradients across the sample area (9, 10). In fact, it is the (time-fluctuating) spatial variations in temperature that induce the convection observed within the molten zone.

That large temperature gradients occur in the experiments of Zerr and Bohler (1), as there must physically be, is evident from their figure 2, which shows a molten zone (now quenched) about 30  $\mu$ m in diameter, surrounded by about 15  $\mu$ m of perovskite that is, in turn, rimmed by untransformed starting material (orthopyroxene). For such an experiment at 62.5 GPa, they report a melting temperature of 5000 ( $\pm$  300) K. The high-pressure melting point is the temperature at the interface at which melt was in contact with crystalline perovskite, here located only 15  $\mu$ m away from the untransformed starting material. Yet it is known that, at pressures above 20 to 25 GPa, pyroxene transforms to perovskite when heated to temperatures exceeding 1000 to 1300 K (18). Therefore, temperature differences of at least 3700 K (5000 K to 1300 K) must have existed over a radial distance of about 15  $\mu$ m. The corresponding temperature gradient of about  $10^8$  to  $10^9$  K per meter is in good accord with our previous theoretical and experimental findings (10, 19).

Somewhat lower temperature gradients may be inferred if Zerr and Bohler were assuming that the temperature is constant across the convecting molten zone. For a Gaussian heat source, as is the case here, the resulting temperature distribution in the dia-

mond cell is often found to be Gaussian, though with some notable exceptions (6, 9, 10). Assuming such a temperature distribution, we can fit Zerr and Bohler's temperature measurement at the center of their hot spot [note 5 in (1)], while constraining the temperature to be less than 1000 to 1300 K in the untransformed pyroxene. Doing so, we obtain a focal-spot diameter comparable to that of Zerr and Bohler [figure 1 in (1)] (20), and a temperature of 3100 ( $\pm$  400) K at a radial distance of 15  $\mu$ m from the hot-spot center, the location of the crystal-melt interface. This value is in good agreement with the melting temperatures reported by our groups and by others for silicate perovskite at 50 to 65 GPa (4, 11, 12, 21).

There could be many reasons for the differences between the Mainz results and other groups' measurements. Among other technicalities, sample configurations, optical components, methods of temperature determination, and criteria for constraining the high-pressure melting curve all differ in detail (22). Nevertheless, it is clear that temperature gradients must be quantified in the CO<sub>2</sub>-laser heated diamond cell (14, 15). These gradients are sensitive to the configuration and properties of the sample and surrounding medium, configurations and properties that change as the sample is taken to successively higher pressures (for example, thinning of the sample under compression) (9, 10). A direct association of the peak temperature with a melting slope, without a characterization of the temperature distribution, is therefore unreliable.

**Dion L. Heinz**

Department of Geophysical Sciences and  
James Franck Institute,  
University of Chicago,  
Chicago, IL 60637, USA

**Elise Knittle**

Earth Sciences Board and  
Institute of Tectonics,  
University of California,  
Santa Cruz, CA 95064, USA

**Jeffrey S. Sweeney**

Department of Geophysical Sciences  
University of Chicago  
**Quentin Williams**

Earth Sciences Board and  
Institute of Tectonics,  
University of California